nature climate change

LETTERS

PUBLISHED ONLINE: 31 AUGUST 2014 | DOI: 10.1038/NCLIMATE2355

Contribution of natural decadal variability to global warming acceleration and hiatus

Masahiro Watanabe[1]*, Hideo Shiogama[2], Hiroaki Tatebe[3], Michiya Hayashi[1], Masayoshi Ishii[4] and Masahide Kimoto[1]

Reasons for the apparent pause in the rise of global-mean surface air temperature (SAT) after the turn of the century has been a mystery, undermining confidence in climate projections[1–3]. Recent climate model simulations indicate this warming hiatus originated from eastern equatorial Pacific cooling[4] associated with strengthening of trade winds[5]. Using a climate model that overrides tropical wind stress anomalies with observations for 1958–2012, we show that decadal-mean anomalies of global SAT referenced to the period 1961–1990 are changed by 0.11, 0.13 and −0.11 °C in the 1980s, 1990s and 2000s, respectively, without variation in human-induced radiative forcing. They account for about 47%, 38% and 27% of the respective temperature change. The dominant wind stress variability consistent with this warming/cooling represents the deceleration/acceleration of the Pacific trade winds, which can be robustly reproduced by atmospheric model simulations forced by observed sea surface temperature excluding anthropogenic warming components. Results indicate that inherent decadal climate variability contributes considerably to the observed global-mean SAT time series, but that its influence on decadal-mean SAT has gradually decreased relative to the rising anthropogenic warming signal.

The change of global-mean SAT during the first decade of the twenty-first century was less than 0.05 °C, indicating a considerably slower rate of warming than during the late twentieth century[3,6]. The causes of this global warming hiatus, which are still under debate, can be categorized into either internal or external processes of the climate system. The principal candidates for external drivers of the hiatus are the weakening of solar activity[7] and increase in stratospheric aerosols[8] plausibly associated with accumulation from minor volcanic eruptions[9]. However, these effects are quantitatively insufficient to explain the warming hiatus. Indeed, satellite measurements of the top of atmosphere (TOA) radiative budgets for 2001–2010 indicate excess energy of about 0.5 W m^{-2} received by the Earth[10], suggesting that the prime cause of the hiatus is internal to the climate system.

Concurrently with the stall of surface warming, despite the energy storage to the system, observational studies have shown evidence that ocean interior warming has occurred continuously[11–15]. This indicates the strengthening of global ocean heat uptake[16], which acts to increase the ocean temperature below 700 m. Whereas historical climate simulations reproduce neither the warming hiatus nor the strengthening of ocean heat uptake during the past decade[3,16], multi-century control simulations with prescribed pre-industrial radiative conditions do reveal intermittent occurrences of pauses in warming and intensification of heat uptake in phase with the Interdecadal Pacific Oscillation (IPO), an inherent low-frequency variability of the Pacific atmosphere–ocean system[17,18].

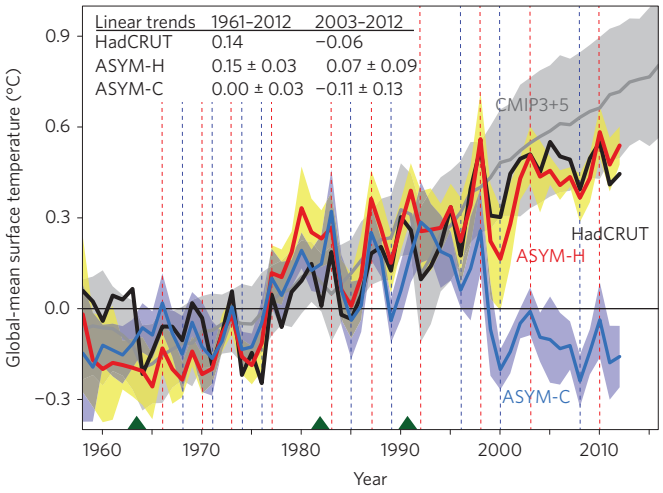

Figure 1 | Observed and simulated change in global-mean surface temperature. Annual-mean time series relative to 1961–1990 mean derived from observations (black), ASYM-H (red) and ASYM-C (blue) experiments. Shading represents ranges of 95% confidence. Linear trends for 1961–2012 and 2003–2012 are denoted at the top. Time series from the combined CMIP3 and CMIP5 models is also shown by the grey curve, with shading representing one standard deviation. Red and blue vertical dashed lines show the occurrence of El Niño and La Niña events, respectively. Three major volcanic eruptions (Agung, El Chichón and Pinatubo) are indicated by green triangles.

Modelling evidence that supports the crucial role of the Pacific atmosphere–ocean variability in the hiatus has been provided by numerical experiments of a climate model in which sea surface temperature (SST) was nudged to observations in the eastern equatorial Pacific since 1861. An ensemble of the historical runs reproduced the hiatus remarkably well[4]. Similarly, prescribing linear trends in tropical wind stresses into a climate model simulated a slowdown of surface warming as well as an increase in heat uptake triggered by the pronounced acceleration of the Pacific trade winds[5].

[1]Atmosphere and Ocean Research Institute, the University of Tokyo, 5-1-5 Kashiwanoha, Kashiwa, Chiba 277-8568, Japan, [2]Center for Global Environmental Research, National Institute for Environmental Studies, 16-2 Onogawa, Tsukuba, Ibaraki 305-8506, Japan, [3]Japan Agency for Marine-Earth Science and Technology, 3173-25 Showa-machi, Kanazawa-ku, Yokohama, Kanagawa 236-0001, Japan, [4]Meteorological Research Institute, Japan Meteorological Agency, 1-1 Nagamine, Tsukuba, Ibaraki 305-0052, Japan. *e-mail: hiro@aori.u-tokyo.ac.jp

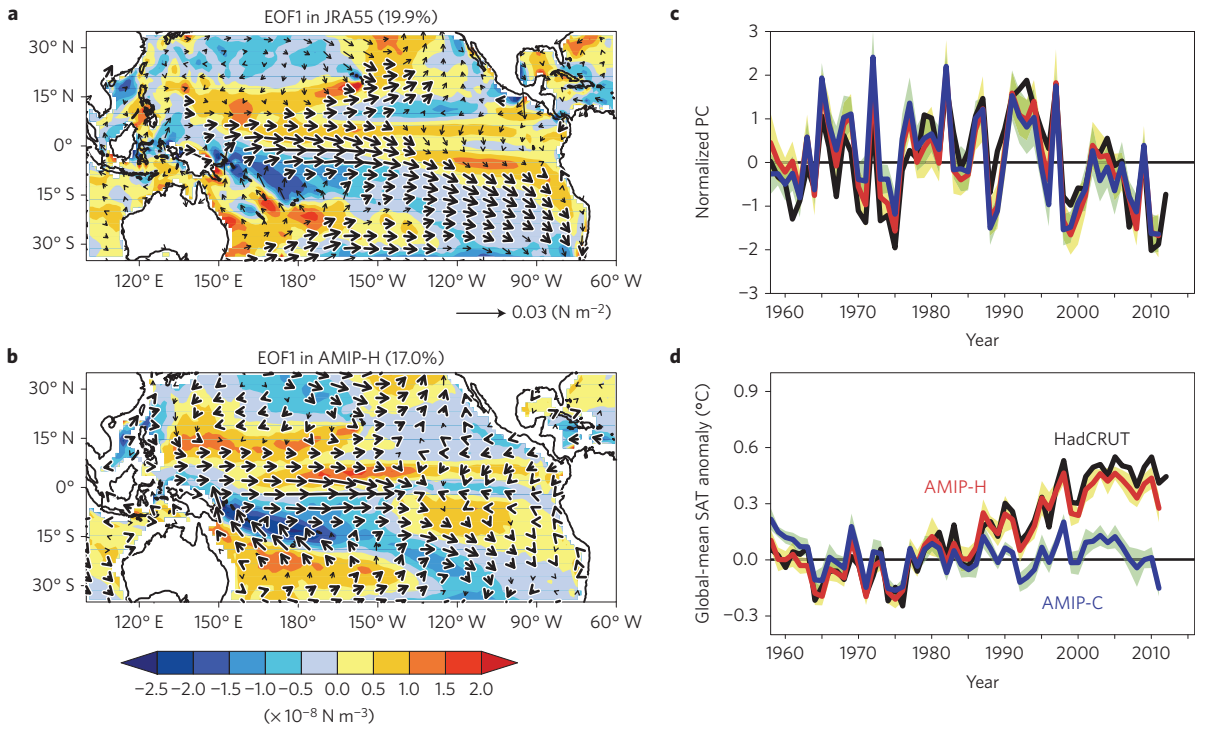

Figure 2 | Leading mode of variability in the tropical Pacific wind stress anomalies. a,**b**, Patterns of EOF1 for JRA55 and AMIP-H runs for 1958–2012. Anomalies significant at the 95% confidence level are thickened. Wind stress curl associated with the EOF patterns is presented by shading. **c**, Principal component (PC) time series associated with the EOF1 for the reanalysis (black), AMIP-H (red) and AMIP-C (blue). Ranges of the 95% confidence interval for the AGCM runs are indicated by shading. **d**, Global-mean SAT anomaly time series for observations, AMIP-H and AMIP-C. The convention is the same as in **c**.

The above modelling results not only suggest an origin of the hiatus attributable to prolonged La Niña-like conditions or negative IPO, but also advocate the usefulness of coupled atmosphere–ocean general circulation model (CGCM) experiments partially driven by observed atmosphere–ocean states. One caveat regarding these experiments is that observations that constrain the CGCM are provided a priori, which hampers quantitative separation of the internally generated and externally forced components of climate change. Such attribution studies have been performed instead using Coupled Model Intercomparison Project (CMIP) multi-model ensembles[19,20]; however, they cannot reproduce correctly the past interannual and decadal fluctuations[3,16].

In this study, we devised a combined modelling approach of using a CGCM forced by observed wind stresses, called partial wind overriding (PWO) experiments, and attribution experiments using an atmospheric general circulation model (AGCM), which provided robust estimates of the extent to which natural decadal fluctuations contributed to the global-mean SAT history over the past five decades, including the period of the global warming hiatus. The model used here is the updated Model for Interdisciplinary Research on Climate version 5 (MIROC5) together with its atmosphere component[21]. For the PWO experiments, surface wind stress anomalies (τ) in MIROC5 were replaced with daily values derived from the 55-year Japanese Reanalysis (JRA55) data set[22] over 30° S–30° N oceans for 1958–2012 (Methods). SST could have been nudged instead, as tropical winds and SST are tied to each other, but the described experiment is advantageous in avoiding artificial heat input into the climate system. A five-member ensemble, called ASYM-H, was branched off from a historical simulation from 1 January 1958. It had slight differences in initial conditions, but identical radiative forcing and other boundary conditions (land use and aerosols) following the CMIP phase 5 (CMIP5; ref. 23) historical and Representative Concentration Pathways 4.5 (RCP4.5) scenario runs before and after 2006. Another set of the five-member ensemble, called ASYM-C, was generated similarly, but with radiative forcing and boundary conditions fixed at the 1850 level.

Figure 1 shows the global-mean SAT time series for ASYM-H and ASYM-C, compared with observations and combined simulations of the 46 CMIP phase 3 (CMIP3; ref. 24) and CMIP5 models (Supplementary Table 1). As in the previous SST-nudged experiment[4], our ASYM-H run reproduces the observed temperature history well (the correlation is $r = 0.89$ for the entire period). Its peaks on interannual time scales are found coincident with the occurrence of El Niño and La Niña events, which are not captured by the CMIP simulations by definition. The linear temperature trend for 2003–2012 is slightly negative in the observations, but slightly overestimated in the ASYM-H run, which might be improved were the natural radiative forcing data updated[25]. A striking feature in Fig. 1 is that ASYM-C generates persistent positive SAT anomalies from the late 1970s to 1999, but negative anomalies beyond; values for the respective decades are 0.11 ± 0.09, 0.13 ± 0.11 and -0.11 ± 0.09 °C for the 1980s, 1990s and 2000s, suggesting a significant contribution of inherent decadal variability. The cooling seen in ASYM-C is clearly reflected by the hiatus in ASYM-H, and the anthropogenic warming during the 1980s and 1990s is amplified by the imposed forcing in τ. A similar comparison between the SST-nudged historical and control experiments was performed in a previous study[4], but, in this work, further quantitative attribution of the history of the global-mean SAT is undertaken. Because there is no input of artificial heat into the system in our PWO experiments, the TOA radiative budget for 2001–2010 is roughly zero in ASYM-C, but it is 0.64 W m^{-2} in ASYM-H, which is close to the latest satellite estimate[10] (Supplementary Fig. 1).

A critical remaining question regards the structure and cause of wind stress variability responsible for the global-mean SAT change

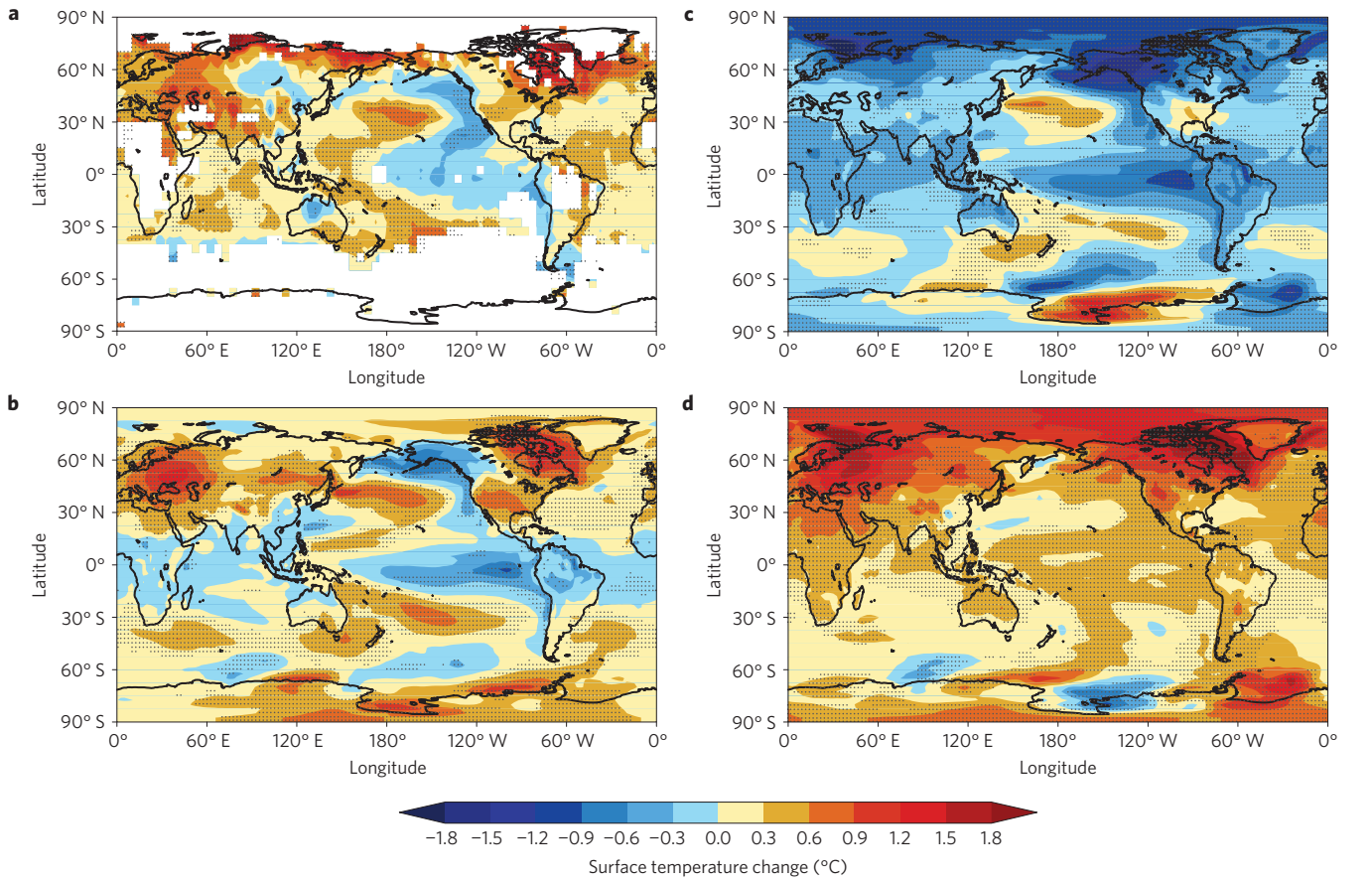

Figure 3 | Observed and simulated SAT change between 1990–1999 and 2001–2012. a,**b**, Observations and ASYM-H, respectively. **c**,**d**, For ASYM-H, ΔT_{ALL} is further decomposed into internal fluctuations (ΔT_{INT}) (**c**) and components externally driven by anthropogenic and natural radiative forcing (ΔT_{EXT}) (**d**). Changes significant at the 95% confidence level are stippled.

on decadal time scales. In particular, if significant anthropogenic influence is embedded within the JRA55 τ, the interpretation of Fig. 1 will be very different. Therefore, the MIROC5 atmospheric component model was used to perform ensemble experiments akin to the Atmospheric Model Intercomparison Project (AMIP) run, driven by observed SST and sea-ice concentrations as well as the radiative forcing data from 1946 to 2012. Thus, the standard ensemble (called AMIP-H) can be compared with another ensemble without involving anthropogenically induced components in SST and boundary conditions (AMIP-C, Methods).

The dominant variability in annual-mean τ anomalies in the observations and the AMIP runs was extracted using an empirical orthogonal function (EOF) analysis to the combined zonal and meridional components of τ over the tropical Pacific of 120° E–100° W, 30° S–30° N (Fig. 2a,b and Supplementary Information). The leading EOF (EOF1), which accounts for 19.9% of the total variance in JRA55 and 17.0% in AMIP-H, represents the fluctuation in the equatorial trade winds. An almost identical EOF1 pattern is obtained from the ASYM-C run and two different observational data sets (Supplementary Fig. 2). Their temporal variability, as represented by the associated principal components (PCs), shows a marked decadal variability signified by weakening trade winds in the 1980s and 1990s and strengthening since the record El Niño in 1997/1998 (Fig. 2c). The weaker trade winds accompany subtropical stress curls that would act to slow the subtropical ocean cell in transporting heat downwards, thus weakening heat uptake[5,15]. The EOF1 includes interannual fluctuations partly associated with the El Niño–Southern Oscillation (ENSO) cycle, but it is separated from the second EOF, which is more distinctive of strong ENSO events, and the ENSO is found non-essential because a similar EOF1 is obtained to the seven-year low-pass filtered τ anomalies (Supplementary Figs 3 and 4).

Unlike the similarity in wind stress variability between the reanalysis and the two AGCM ensembles, the global-mean SAT time series illustrates a clear difference between them; AMIP-H reproduces the observations, but AMIP-C has no global warming signal, as ensured by the experimental design (Fig. 2d). Moreover, the decadal τ variability represented by the EOF1 has a different spatial structure and is much greater than the anthropogenic trend pattern obtained from differences between AMIP-H and AMIP-C (Supplementary Fig. 5). It is therefore concluded that the dominant wind stress fluctuation that could have driven decadal SAT changes in ASYM-C is natural variability without detectable anthropogenic influence. This conclusion is further supported by another PWO experiment similar to ASYM-C, but without linear trends for 1958–2012 in the JRA55 τ (see Methods and Supplementary Fig. 6).

Using the PWO experiments, the SAT changes between the hiatus period (2001–2012) and a previous decade (1990–1999) in ASYM-H, denoted as ΔT_{ALL}, were decomposed into internal variability (ΔT_{INT}) and externally forced components (ΔT_{EXT}) due both to anthropogenic forcing and natural radiative forcing by solar activity and volcanoes (Methods). The observed cooling in the eastern half of the Pacific and warming in the western Pacific, as well as over high-latitude continents, are represented well by ΔT_{ALL}, but discrepancies are seen in the tropical Atlantic and Indian Ocean (compare Fig. 3a with 3b). The pattern of ΔT_{ALL} occurs because of compensation between ΔT_{INT} and ΔT_{EXT}—the former leading to a

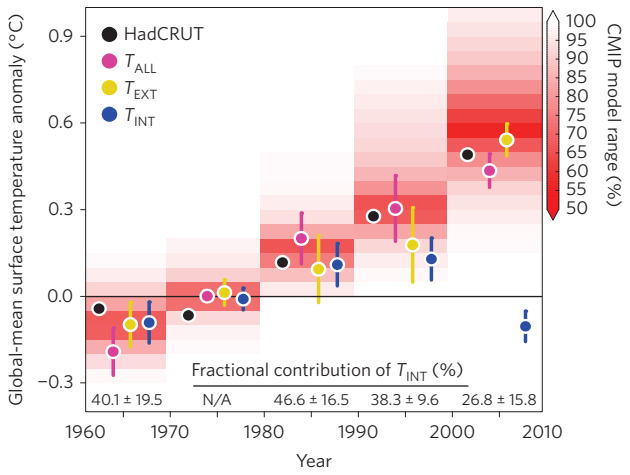

Figure 4 | Contribution of internal and external components to decadal-mean SAT anomalies relative to the 1961–1990 mean. Circles indicate the decadal SAT anomaly from observations (black), ΔT_{ALL} (pink), ΔT_{EXT} (yellow) and ΔT_{INT} (blue) with ranges of the 95% confidence interval denoted by vertical error bars. Red shading indicates the probabilistic range of decadal SAT anomalies calculated from 46 CMIP models. The fractional contribution of ΔT_{INT} to ΔT_{ALL} (absolute value as percentage) for each decade is presented at the bottom. The fraction for 1971–1980 is not available because ΔT_{ALL} is close to zero.

worldwide cooling (Fig. 3c). In particular, the strong polar cooling is dominated by northerly advection over Alaska associated with the remote teleconnection from the tropical Pacific[18].

The externally forced component is statistically most significant and shows the well-known anthropogenic signals of the polar amplification and increasing land–sea contrast (Fig. 3d). The cooling effect of volcanic forcing, dominated by the Pinatubo eruption[9] in the 1990s, is included in ΔT_{EXT}, which is overlaid with the anthropogenic warming signal. The contrast between ΔT_{INT} and ΔT_{EXT} is also evident in the zonal-mean ocean temperature (Supplementary Fig. 7). Accompanied by ΔT_{INT}, subsurface warming occurs beneath the subtropical thermocline, indicative of circulation spin-up in the 2000s, whereas the surface warming signal of ΔT_{EXT} penetrates into deeper layers in northern high latitudes. The difference in warming structure of the ocean interior implies different mechanisms operating between inherent variability and forced response.

Returning to the global-mean quantities, the above decomposition was then applied to the decadal-mean SAT anomaly (Fig. 4). Considering that the probabilistic estimate of the 46 CMIP model runs provides a range of uncertainty, all the components except ΔT_{INT} for the recent two decades reside within it. However, ΔT_{EXT} tends to be lower than the observations during the 1980s and 1990s, but higher in the 2000s. This indicates that, consistent with Fig. 1, ΔT_{INT} amplifies or suppresses the anthropogenic warming signal. The fractional contribution of ΔT_{INT} to ΔT_{ALL} for the three decades was estimated as 46.6%, 38.3% and 26.8%, respectively (confidence intervals presented in Fig. 4). The lowest contribution during the hiatus period was due to the increase of ΔT_{EXT}, which is not contradictory to the dominant effect of the inherent variability to reduce the warming tendency. The above estimate demonstrates the considerable influence of internal variability to the decadal-mean SAT over recent periods, but suggests that the influence relative to the anthropogenic signal will decrease in the future. Precisely, an anthropogenic component representing the weakening of the Walker circulation[26,27] may be included in the JRA55 τ (Supplementary Fig. 6). However, the longer trend of a trade deceleration is opposite to the acceleration for the recent 15 years responsible for the global-mean cooling in ASYM-C (Fig. 1), which is due plausibly to natural variability.

The PWO experiments in this work provide a novel framework for attributing past climate changes with higher accuracy than attributions based on CMIP simulations. The reproducibility of past interannual and decadal climate variability by the PWO experiments would also have advantages in regional climate change attribution, not only for temperature, but also for precipitation and other climate variables that have greater impact on human society.

Methods

Observational data sets. We used the Hadley Centre–Climate Research Unit combined land SAT and SST (HadCRUT) version 4 (ref. 28) and JRA55 reanalysis from January 1958 onwards[22]. When calculating global-mean SAT from all of the numerical simulations, we used grid points where HadCRUT data were available in each year. To verify low-frequency variability in the JRA55 wind stress anomalies, we also used two different data sets (Supplementary Information).

CGCM PWO experiments. For performing our PWO experiments, we used a state-of-the-art climate model called MIROC5 (ref. 21), with updates to ocean components (Supplementary Information), and a baseline set of historical and scenario experiments performed for 1850–2100 following CMIP5 protocols. In the ASYM-H and ASYM-C experiments, anomalies of τ relative to model climatology were replaced with τ anomalies interpolated from reanalysis-derived daily fields at each time step over tropical oceans. ASYM-H used radiative forcing identical to the baseline experiments for 1958–2012, whereas ASYM-C used radiative forcing fixed at 1850 values. Additionally, we repeated ASYM-C runs, but with reanalysis-derived τ anomalies from which the linear trends for 1958–2012 had been subtracted. A comparison of this ensemble, called ASYM-CNT, and ASYM-C revealed little difference, supporting our conclusion (Supplementary Information).

AGCM attribution experiments. The radiative forcing given to ASYM-H was also applied to AMIP-H for 1946–2012, in which monthly observations of SST and sea-ice concentrations from the Hadley Centre sea ice and SST version 1 (ref. 29) were prescribed. Anthropogenic forcing was not given in AMIP-C as in ASYM-C, and human-induced signals on SST and sea ice, estimated in advance using CGCM attribution experiments, were removed[30] (Supplementary Information). Both AMIP-H and AMIP-C consist of ten-member runs for each.

Decomposition of internally and externally driven temperature changes . Attribution of decadal temperature change due to internal climate variability and externally forced components was expressed as $\Delta T_{ALL} = \Delta T_{INT} + \Delta T_{EXT}$, where ΔT_{ALL} and ΔT_{INT} are anomalies in ASYM-H and ASYM-C, respectively, and ΔT_{EXT} is their difference. This separation might potentially contain errors that arise from an assumption that the natural forcing of volcanoes and solar activity do not have decadal-scale imprints in the JRA55 τ anomalies that drive ASYM-C.

Received 23 May 2014; accepted 24 July 2014;
published online 31 August 2014

References

1. Tollefson, J. The case of the missing heat. *Nature* **505,** 276–278 (2014).
2. Trenberth, K. E. & Fasullo, J. T. An apparent hiatus in global warming? *Earth's Future* **1,** 19–32 (2013).
3. Fyfe, J. C., Gillett, N. P. & Zwiers, F. W. Overestimated global warming over the past 20 years. *Nature Clim. Change* **3,** 767–769 (2013).
4. Kosaka, Y. & Xie, S-P. Recent global-warming hiatus tied to equatorial Pacific surface cooling. *Nature* **501,** 403–407 (2013).
5. England, M. H. *et al.* Recent intensification of wind-driven circulation in the Pacific and the ongoing warming hiatus. *Nature Clim. Change* **4,** 222–227 (2014).
6. Easterling, D. R. & Wehner, M. F. Is the climate warming or cooling? *Geophys. Res. Lett.* **36,** L08706 (2009).
7. Kaufmann, R. K., Kauppi, H., Mann, M. L. & Stock, J. H. Reconciling anthropogenic climate change with observed temperature 1998–2008. *Proc. Natl Acad. Sci. USA* **108,** 11790–11793 (2011).
8. Solomon, S. *et al.* The persistently variable 'background' stratospheric aerosol layer and global climate change. *Science* **333,** 866–870 (2011).
9. Santer, B. D. *et al.* Volcanic contribution to decadal changes in tropospheric temperature. *Nature Geosci.* **7,** 185–189 (2014).
10. Loeb, N. G. *et al.* Observed changes in top-of-the-atmosphere radiation and upper-ocean heating consistent within uncertainty. *Nature Geosci.* **5,** 110–113 (2012).

11. Domingues, C. M. *et al.* Improved estimates of upper-ocean warming and multi-decadal sea-level rise. *Nature* **453,** 1090–1094 (2008).
12. Levitus, S. *et al.* World ocean heat content and thermosteric sea level change (0–2000 m), 1955–2010. *Geophys. Res. Lett.* **39,** L10603 (2012).
13. Lyman, J. M. *et al.* Robust warming of the global upper ocean. *Nature* **465,** 334–337 (2012).
14. Gleckler, P. J. *et al.* Human-induced global ocean warming on multidecadal timescales. *Nature Clim. Change* **2,** 524–529 (2012).
15. Balmaseda, M. A., Trenberth, K. E. & Källén, E. Distinctive climate signals in reanalysis of global ocean heat content. *Geophys. Res. Lett.* **40,** 1754–1759 (2013).
16. Watanabe, M. *et al.* Strengthening of ocean heat uptake efficiency associated with the recent climate hiatus. *Geophys. Res. Lett.* **40,** 3175–3179 (2013).
17. Meehl, G. A., Arblaster, J. M., Fasullo, J. T., Hu, A. & Trenberth, K. E. Model-based evidence of deep-ocean heat uptake during surface-temperature hiatus periods. *Nature Clim. Change* **1,** 360–364 (2011).
18. Meehl, G. A., Hu, A., Arblaster, J. M., Fasullo, J. & Trenberth, K. E. Externally forced and internally generated decadal climate variability associated with the Interdecadal Pacific Oscillation. *J. Clim.* **26,** 7298–7310 (2013).
19. Meehl, G. A., Hu, A. & Santer, B. D. The mid-1970s climate shift in the Pacific and the relative roles of forced versus inherent decadal variability. *J. Clim.* **22,** 780–792 (2009).
20. Stott, P. A. *et al.* Detection and attribution of climate change: A regional perspective. *WIREs Clim. Change* **1,** 192–211 (2010).
21. Watanabe, M. *et al.* Improved climate simulation by MIROC5: Mean states, variability, and climate sensitivity. *J. Clim.* **23,** 6312–6335 (2010).
22. Ebita, A. *et al.* The Japanese 55-year Reanalysis 'JRA-55': An interim report. *SOLA* **7,** 149–152 (2011).
23. Taylor, K. E. *et al.* An overview of CMIP5 and the experiment design. *Bull. Am. Meteorol. Soc.* **93,** 485–498 (2012).
24. Meehl, G. A. *et al.* The WCRP CMIP3 multimodel dataset: A new era in climate change research. *Bull. Am. Meteorol. Soc.* **88,** 1383–1394 (2007).
25. Schmidt, G. A., Shindell, D. & Tsigaridis, K. Reconciling warming trends. *Nature Geosci.* **7,** 158–160 (2014).
26. Vecchi, G. A. *et al.* Weakening of tropical Pacific atmospheric circulation due to anthropogenic forcing. *Nature* **441,** 73–76 (2006).
27. Tokinaga, H., Xie, S-P., Deser, C., Kosaka, Y. & Okumura, Y. Slowdown of the Walker circulation driven by tropical Indo-Pacific warming. *Nature* **491,** 439–444 (2012).
28. Morice, C. P., Kennedy, J. J., Rayner, N. A. & Jones, P. D. Quantifying uncertainties in global and regional temperature change using an ensemble of observational estimates: The HadCRUT4 data set. *J. Geophys. Res.* **117,** D08101 (2012).
29. Rayner, N. A. *et al.* Global analyses of sea surface temperature, sea ice, and night marine air temperature since the late nineteenth century. *J. Geophys. Res.* **108,** 4407 (2003).
30. Shiogama, H. *et al.* An event attribution of the 2010 drought in the South Amazon region using the MIROC5 model. *Atmos. Sci. Lett.* **14,** 170–175 (2013).

Acknowledgements

This work was supported by the Grant-in-Aid 26247079 and the Program for Risk Information on Climate Change (SOUSEI program) from the Ministry of Education, Culture, Sports, Science and Technology (MEXT), Japan.

Author contributions

M.W. led the research and wrote the paper. M.W., H.S. and M.H. performed the experiments. H.T. and M.I. prepared part of the data and model. M.K. contributed to improving the analysis and interpretation. All the authors discussed the results and commented on the manuscript.

Additional information

Supplementary information is available in the online version of the paper. Reprints and permissions information is available online at www.nature.com/reprints. Correspondence and requests for materials should be addressed to M.W.

Competing financial interests

The authors declare no competing financial interests.